ChemCatChem

Research Article
doi.org/10.1002/cctc.202200732

Chemistry Europe
European Chemical Societies Publishing

www.chemcatchem.org

Nanostructured Sonophotocatalysts for spatially controlled inertial cavitation towards energy-efficient sonochemistry

Umesh S. Jonnalagadda,[a] Qianwenhao Fan,[a] Xiaoqian Su,[a] Wen Liu,*[a] and James J. Kwan*[b]

Catalytic nanomaterials have been demonstrated to enhance sonochemical processing through interactions with inertial cavitation events. Typically, sonochemistry generates inertial cavitation events directly from the solvent, which results in spatially uncontrolled cavitation events with limited interaction with the catalytic active site. These high intensity acoustic fields also result in thermal effects and side reactions, which may further influence chemical yields and selectivity. Herein, we report on ultrasound-responsive structured AuPd/TiO_2 open nanoshells (TONs) to surface-stabilize gas bubbles for promoting cavitation events in the vicinity of catalytic active site. These exogenous bubbles trapped on catalytic active sites readily cavitate to produce free radicals for chemical reactions. Our findings indicate a positive trend between cavitation and benzaldehyde production in the presence of our AuPd/TONs. In contrast, nanostructures without gas-stabilization demonstrate reduced sonochemical conversion, suggesting the catalytic potential of nanostructuring photocatalytic materials to function as both cavitation agents and photo-oxidative catalysts, or photocatalytic nanostructure (PCN).

Introduction

The chemical effects of ultrasound are typically derived from indirect phenomena initiated by the acoustic field.[1] The primary driving force of sonochemical conversion is inertial cavitation,[2] an acoustic phenomenon in which a high intensity acoustic field nucleates a gas bubble or vapor cavity. This bubble then experiences a rapid expansion before eventually undergoing inertial collapse.[3] This collapse violently changes the local physicochemical environment, inducing pyrolysis, heating, microjetting, and sonoluminescence.[3–4] It is in part the pyrolysis of water (also known as sonolysis) during inertial cavitation that generates free radicals, e.g., reactive oxygen species (ROS), under macroscopically ambient conditions without any chemical additive or other external stimuli (e.g., light or electric potential). Sonolysis and other cavitation phenomena have also been demonstrated in nonaqueous solvents, e.g., alkanes, acetonitrile, and alcohols.[4f] Thus, sonochemistry has shown potential in a broad spectrum of applications including polymer synthesis,[5] biomedical therapies,[6] and selective oxidation.[7]

Given that bubble nucleation is a stochastic process and is spatiotemporally random in homogenous fluids,[4b] conventional sonochemistry often relies on continuous input of high-intensity acoustic energy to generate sufficient inertial cavitation events throughout the fluid medium to afford satisfactory reaction rates. However, prolonged continuous wave irradiation can lead to undesirable secondary effects[2b] and side reactions,[5] which are also dependent on the driving frequency of the ultrasonic irradiation. For instance, during sonochemical polymerization, low frequency ultrasound (20–100 kHz)[8] could limit the growth of the polymer chain owing to the higher fluid shear stress brought by low frequency cavitation.[5] Comparatively, the work by Ashokkumar and co-workers demonstrated that cavitation events by higher frequency ultrasound (> 200 kHz) permitted greater radical generation than lower frequencies,[3] and enabled rapid sonochemical polymerization.[2b,5,9] Unfortunately, these acoustic waves are also more readily attenuated by fluids,[10] leading to thermal effects with prolonged irradiation.[4d] Furthermore, the reactor design can influence the conversion of electrical energy to cavitation energy, ultimately affecting the energy efficiency associated with radical generation in sonochemical reactors.[3] For example, the cavitation clouds generated near the transducer face and reactor lumen at high pressures could attenuate the sound field and hinder the energy transfer for more effective radical generation.[3]

To improve the efficiency of sonochemical processing, heterogeneous catalysts have been employed to interact with the acoustic wave and cavitation events. For example, piezoelectric catalysts have been demonstrated to generate radicals through direct interaction with the acoustic field and cavitation events,[11] while photosensitizers have been used to interact with sonoluminescence light to enhance the generation of radicals in the fluid media.[6a,12] Despite the advent of hetero-

[a] Dr. U. S. Jonnalagadda, Q. Fan, Dr. X. Su, Prof. W. Liu
School of Chemical and Biomedical Engineering
Nanyang Technological University
62 Nanyang Drive
Singapore, 637459, Singapore (Singapore)
E-mail: wenliu@ntu.edu.sg
[b] Prof. J. J. Kwan
Department of Engineering Sciences
University of Oxford
Parks Rd
Oxford OX1 3PJ (UK)
E-mail: james.kwan@eng.ox.ac.uk

Supporting information for this article is available on the WWW under https://doi.org/10.1002/cctc.202200732

genous catalysts for improved sonochemical activity, the stochastic nature of bubble nucleation means that sonoluminescence and sonolysis-derived radicals generated by inertial cavitation may not always interact with catalytically active sites. This in turn limits the productivity of the heterogeneously catalyzed sonochemistry, as depicted in Figure 1a.

Interestingly for ultrasonic imaging, exogenous cavitation nuclei have been utilized to permit cavitation-mediated contrast enhancement at low acoustic intensities (mechanical index <1.1) to minimize off-site physiological damage from stochastic cavitation events.[4b] These cavitation nuclei, or cavitation agents, were microbubble-based systems and have since been demonstrated to interact with photosensitive chemotherapeutics for radical generation *in vitro*[4e] and *in vivo*.[13] More recently, it has been reported that nanostructured polymeric particles with surface bubbles could function as effective cavitation agents, i.e. materials that promote acoustic cavitation.[4b,14] Notably, these reports demonstrated the generation of inertial cavitation using ultrasonic irradiation pulsed at low duty cycles ($<10\%$), as opposed to continuous wave irradiation commonly used in sonochemistry (i.e., 100% duty cycle). This distinction is important as it indicates that cavitation agents could effectively reduce the energy threshold for cavitation events and presents a viable strategy for improving the energy efficiency of sonochemical systems.

Herein, we prepared nanostructured AuPd/TiO_2 particles for the sonocatalytic oxidation of benzyl alcohol (BnOH) to benzaldehyde using pulsed ultrasound. TiO_2 was selected as it is a well-known material for photo- and sonocatalysis,[4c,15] and our nanostructure (TiO_2 open nanoshell, or TON) permits gas stabilization onto the catalyst surface, where cavitation events may occur exclusively, as opposed to stochastically in the fluid media.[16] In doing so, sonoluminescence can be efficiently absorbed by the photoactive surface of TiO_2, leading to the facile generation of ROS, e.g., hydroxyl radicals and singlet oxygen via water sonolysis and sonoluminescence-induced photolysis (see Figure 1b).[4c,15b,16] These ROS are then utilized by the AuPd nanoalloys supported on the TiO_2 nanostructure (AuPd/TON). The AuPd nanoalloys serve as the active sites for the catalytic oxidation of alcohols to aldehydes,[17] in this case, the oxidation of benzyl alcohol to benzaldehyde. We experimentally show that gas-trapping AuPd/TONs are highly responsive to pulsed ultrasound, leading to the rapid oxidation of BnOH. In an aqueous solution of 4.8 mM BnOH and 24 mM H_2O_2, the AuPd/TON-facilitated sonochemistry achieved a reaction rate of $0.18 \pm 0.03\ \mu mol\,L^{-1}\,s^{-1}$ under pulsed ultrasound of 1.1 MHz at a 33% duty cycle for 10 minutes. Comparatively, ultrasonic irradiation of the reaction solution without any photocatalytic nanostructure (PCN) demonstrated a much slower reaction rate of $0.051 \pm 0.02\ \mu mol\,L^{-1}\,s^{-1}$. When the gas stabilization function of the AuPd/TON PCN was chemically neutralized to create degassed AuPd/TONs, the reaction rate was reduced to $0.046 \pm 0.003\ \mu mol\,L^{-1}\,s^{-1}$. When further manipulating the acoustic parameters to investigate chemical yields between 0–10% duty cycles, we observed gas-trapping AuPd/TONs to have consistently performed better than degassed AuPd/TONs. Compared to the homogeneous catalysts used in sonochemistry,[18] the PCN is recoverable after reactions, making the overall process more economic and resource-efficient.[19]

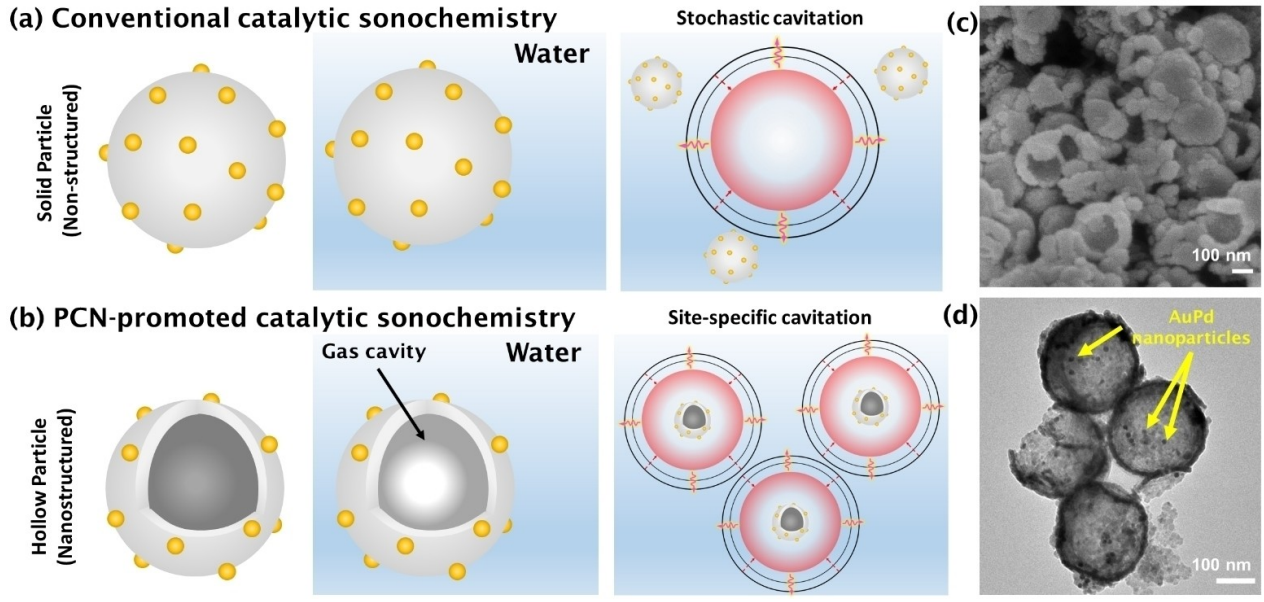

Figure 1. Schematic illustration of cavitation events by ultrasonic exposure. (a) Heterogenous catalysts can function as a nucleation site for cavitation, but the lack of gas-stabilization results in limited cavitation at the catalyst site. (b) By nanostructuring the catalyst, PCNs permit site-specific cavitation on the particle surface sonocatalytic oxidation reactions. The morphology of AuPd loaded TiO_2 open nanoshells (AuPd/TON) was assessed by (c) SEM and (d) TEM. Scale bars for Figure 1c and d are 100 nm.

Results and Discussion

A characterizing feature of solid cavitation agents is a rough surface on which gas bubbles can be stabilized.[14,16,20] We have previously demonstrated nanostructured TiO_2 particles as dual-modal photocatalytic nanostructures and cavitation agents (dubbed TONs) and herein, we extend the application of the structures further through surface deposition of AuPd nanoparticles to form AuPd/TONs. In addition to providing active sites for alcohol oxidation,[17] AuPd may also function as a co-catalyst to facilitate the efficient separation of photogenic charge carriers (due to sonoluminescence) to improve the efficiency of photocatalysis.[21] The SEM images of the TON and AuPd/TON samples (Figure 1c) confirm the open nanoshell morphology with an average size of ~210 nm, which is essential for promoting and localizing cavitation. Additionally, the TEM images (Figure 1d) show that the AuPd nanoparticles, with mean particle size ~10 nm, are well dispersed on TON. TEM-EDX elemental mapping (Figure S1) further confirms the good dispersion of the AuPd nanoparticles over the TONs. The spatial overlap of EDX signals of Au and Pd at locations with clear presence of noble metal nanoparticles suggests that the two components form a well-mixed alloy. The co-catalyst composition and loading concentration on the TONs was determined by inductively coupled plasma-optical emission spectroscopy (ICP-EOS), which shows AuPd/TONs to have a metal loading of approximately 1.2 wt% (Table S1). Pd:Au mass ratio of the noble metal alloy was found to be a 1:10. The particles before and after AuPd deposition were examined by XRD, which confirmed the absence of any change to the crystal structure due to metal deposition (Figure S2). TiO_2 in both TONs and AuPd/TONs primarily exhibit the anatase structure (space group = $I4_1/amd$). The lack of any diffraction peak of AuPd confirms their low loading and small particle size.

Acoustic Response and Cavitation Behavior of AuPd/TONs

As it is understood that the surface properties of particles can influence their hydrophobicity and, thus, propensity to stabilize gas cavities, we next assessed the acoustic response of the PCNs and their propensity to nucleate cavitation through a range of peak negative pressure amplitudes using a center frequency of 1.1 MHz (Figure S3). In order to validate the influence of AuPd co-catalyst on the acoustic response of the PCNs, we compared the cavitation threshold of AuPd/TONs (minimum peak negative pressure for 50% cavitation) to unmodified TONs and also wetted AuPd/TONs (dubbed degassed AuPd/TONs) to validate the acoustic response from the particles as a result of gas stabilization (Table 1).

Table 1. Average cavitation threshold pressures of PCNs. $\bar{x} \pm$ SEM, $n = 3$.

Particle	Cavitation Threshold (MPa)
TONs	4.5 ± 0.2
AuPd/TONs	3.0 ± 0.3
Degassed AuPd/TONs	6.4 ± 0.3

Unmodified TONs exhibited a cavitation threshold at 4.5 ± 0.2 MPa peak negative pressure, which corroborates with previous findings.[16] Interestingly, AuPd/TONs were found to have a much lower cavitation threshold (3.0 ± 0.3 MPa) than the unmodified TONs. This change may be explained by a decrease in surface wettability (i.e., increased hydrophobicity) upon the deposition of AuPd nanoparticles. Because gas trapping in part relies on the PCN having a hydrophobic surface,[22] surface modification will affect the stability of gas bubbles on the particle surface. In this sense, a more hydrophobic surface could stabilize more gas bubbles and promote cavitation at lower pressures. To verify this rationale, the AuPd/TONs particles were washed by ethanol to "neutralize" the surface hydrophobicity and bubble stability; this sample is denoted degassed AuPd/TONs. While it is difficult to entirely remove all gas bubbles from a surface[23] (even under vacuum),[24] the ethanol-washing will minimize gas stabilization on the particle surface. The influence of the washing is evident as degassed AuPd/TONs showed a substantially increased cavitation threshold (6.4 ± 0.3 MPa) compared to the threshold of 3.0 ± 0.3 MPa prior to degassing. The above observation confirms that the increased cavitation response exhibited by the AuPd/TONs is likely due to the increased surface hydrophobicity upon deposition of AuPd nanoparticles. In addition to the acoustic response profile illustrated in Figure S3, we validated the frequency content above and below the cavitation thresholds for our PCNs (Figure S4). Here, we observed that prominent broadband noise at and above the cavitation threshold, which is indicative of inertial cavitation.[14a,25] From this, we can confirm that the deposition of AuPd nanoparticles onto the TONs not only improved the acoustic response of the PCNs, but also promoted inertial cavitation, which is of primary importance to radical generation and oxidative processes in macroscopically ambient conditions.

In addition to the initial intensity of inertial cavitation (as quantified by the broadband noise shown in Figure S4), the time for which the PCNs can sustain their cavitation response is also important, as it dictates the duration over which the PCNs remain fully functional during continuous operations. To this end, we investigated the duration of cavitation of the PCNs over 10 minutes of irradiation at a 33% duty cycle and 6.8 MPa peak negative pressure. This peak negative pressure selected is above the cavitation threshold of all the cavitation agents studied (see Table 1), but below the requirement for cavitation in pure water. As such, inertial cavitation would exclusively occur on the PCNs, i.e., the cavitation events are localized on the PCNs. From the results shown in Figure S5a, the mixtures containing AuPd/TONs at 0.5–1.5 mg/mL exhibited consistently intense inertial cavitation over 10 min of pulsed ultrasound irradiation. In comparison, the mixtures containing degassed AuPd/TONs showed significantly weaker inertial cavitation (Figure S5b). In particular, the experiments with 0.5–1.0 mg/mL degassed AuPd/TONs showed decaying broadband cavitation response over time, suggesting that the degassed AuPd/TONs could not sustain their PCN functionality due to weakened surface hydrophobicity. In all cases, solutions without PCNs (i.e., BnOH only) were observed to not have exhibited any change in acoustic intensity and, thus, cavitation events.

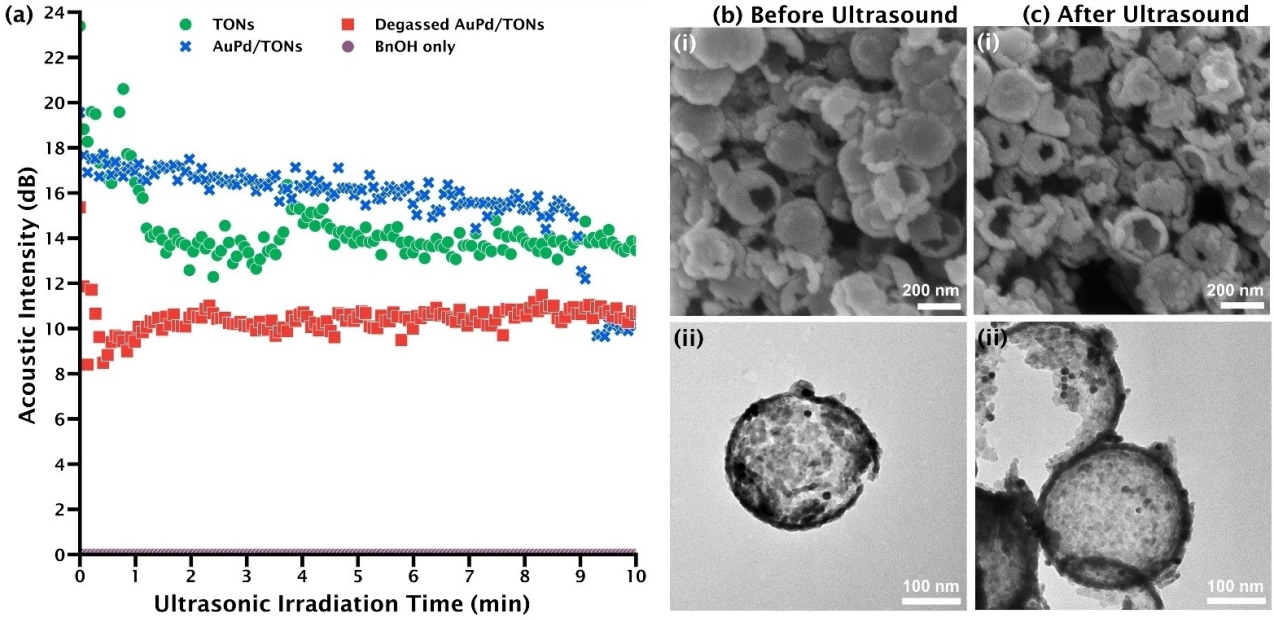

Figure 2. (a) Representative data demonstrating the efficacy of different PNCs to sustain broadband cavitation was quantified over a 10-minute ultrasonic irradiation period with a 33% duty cycle (1.1 MHz and 6.8 MPa). For clarity, data points are depicted every 50 pulses. Representative images of PCNs (b) before and (c) after ultrasound irradiation. (i) SEM micrographs did not indicate significant change to the particle structure and (ii) TEM imaging further validated presence of AuPd cocatalyst on the TONs following ultrasonic irradiation. Scale bars in bi and ci denote 200 nm. The scale bars in bii, cii denote 100 nm.

We next compared the duration of cavitation events of all the cavitation agents (viz. TONs, AuPd/TONs and degassed AuPd/TONs) to verify the influence of the PCNs on sustaining localized inertial cavitation, as shown in Figure 2a. Over the 10 min irradiation, both the fresh AuPd/TONs and unmodified TONs showed consistent cavitation response at 6.8 MPa peak negative pressure, whereas the cavitation intensity of degassed AuPd/TONs dropped to half of its initial value after ~2 min. This result indicates that gas-trapping by a relatively hydrophobic surface is essential for the PCNs to function in practical scenarios where long bubble lifetimes are desired over continuous ultrasound irradiation. According to SEM images shown in Figure 2bi and Figure 2ci, the morphology of the AuPd/TONs prior to and following ultrasonic irradiation was comparable. Additionally, AuPd particles remain uniformly dispersed over the surfaces of TONs after sonication, as shown in the TEM images in Figure 2bii and Figure 2cii. Therefore, the electron microscopy images suggest that the PCNs are structurally stable and suitable for sonochemical applications over prolonged ultrasonic irradiation periods.

Sonochemical Oxidation of Benzyl Alcohol with AuPd/TONs

Preliminary investigations into PCN-mediated sono-oxidation were carried out using 0–1.5 mg/mL AuPd/TONs to facilitate the catalytic oxidation of benzyl alcohol (BnOH) to benzaldehyde (BzA) under 10 minutes of ultrasonic irradiation using a 6.8 MPa peak negative pressure, 10 ms pulse duration, and 33% duty cycle at a center frequency of 1.1 MHz. By controlling the dose of ultrasonic radiation, we operated in the low conversion regime, where the apparent reaction rates are less hindered by mass transfer resistance or chemical equilibrium. In each reaction, hydrogen peroxide (H_2O_2) was used as an oxidant, which was added to the reaction mixture containing 4.8 mM BnOH at an equivalence ratio of 5:1. The excess of H_2O_2 was to ensure the sufficient supply of oxidant in a closed, unagitated environment.[18,26] In all experiments, benzaldehyde was the only oxidation product detected.

The experimental data, as shown in Figure 3 and Table S2, indicate that the rate of benzaldehyde production increased with the PCN concentration, from 0.05 μmol L^{-1} s^{-1} (without any PCN) to 0.2 μmol L^{-1} s^{-1} (with a PCN concentration of 1.5 mg/

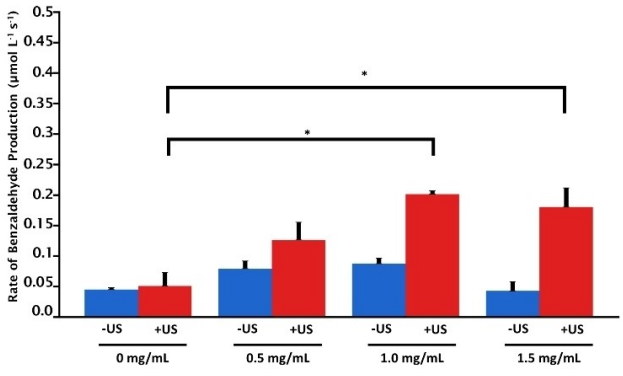

Figure 3. Benzyl alcohol conversion to benzaldehyde over 10 minutes ultrasound irradiation at a 33% duty cycle and 6.8 MPa (+US). Benzyl alcohol conversion ultrasound over the same irradiation period is denoted as −US. AuPd/TONs concentration varied from 0–1.5 mg/mL, n = 3, $\bar{x}$ + SEM, *$p < 0.05$.

mL) under identical ultrasound irradiation. In the absence of ultrasound, the background activities of the working solution (4.8 mM BnOH and 5-mole equivalent of H_2O_2), with or without PCNs, was measured to be 0.045–0.087 $\mu mol\,L^{-1}\,s^{-1}$, which is significantly lower than that of PCN-mediated catalytic sonochemistry. Furthermore, the use of PCNs without ultrasonic irradiation did not result in any statistically significant increase in rates as compared to the BnOH only control group (without any catalyst, no ultrasound (Figure 3). Given this, it can be reasoned that neither the peroxide content in the working solution nor the PCNs alone, without ultrasonic irradiation, exhibits prominent catalytic activity to oxidize BnOH to BzA. Comparatively, we observed AuPd/TONs with ultrasonic irradiation to exhibit a statistically significant increase of 3.5 folds in the reaction rate when the PCN concentration increased from 0 mg/mL to 1.5 mg/mL. Therefore, the ultrasound-driven, PCN-facilitated inertial cavitation is essential for activating the catalytic oxidation of benzyl alcohol under the present set of experimental parameters used.

Validating the Role of Inertial Cavitation on Catalytic Oxidation of Benzyl Alcohol with AuPd/TONs

Despite inertial cavitation being the driving force for sonochemistry, it is rarely quantified in the relevant literature. Here, we performed an indirect measure of the intensity of inertial cavitation by analyzing the received PCD signal at the broadband frequencies, which is proportional to the inertial cavitation energy. As such, the rate of received broadband signal energy was used to determine the correlation between the apparent rates of reaction and inertial cavitation, where the latter depends on PCN concentration, duty cycles and ultrasound irradiation time. As shown in Figure 4, the AuPd/TONs concentration correlates positively to the received broadband PCD signal energy. Correspondingly, the rate of benzaldehyde production was observed to increase proportionally with the catalyst concentration and, likewise, the inertial cavitation energy. To validate this trend as a result of inertial cavitation generated by the AuPd/TON PCNs, we next repeated this study using the degassed AuPd/TONs. Here, the degassed AuPd/TONs exhibit reduced cavitation, with no observable increase in benzaldehyde production rate with increased catalyst concentration (Figure 4). This is likely a result of the reduced capacity of the degassed PCNs to stabilize gas bubbles, thereby limiting their efficacy for site-controlled cavitation at the catalytic active site. Therefore, only the AuPd/TON PCNs enhance inertial cavitation, which is in turn promoted the rates of benzaldehyde production.

Based on the preliminary experimental results (*vide supra*), all subsequent sonochemistry experiments were performed at a catalyst concentration of 1.5 mg/mL. To better understand how pulsed ultrasound could enhance the efficiency of PCN-assisted sonochemistry, we investigated the influence of ultrasound on-time on BzA yield over a duration of 30 minutes using a 0%, 5%, or 10% duty cycle with a lower pulse duration of 10 ms; the results are also shown in Figure S6. These lower duty cycles

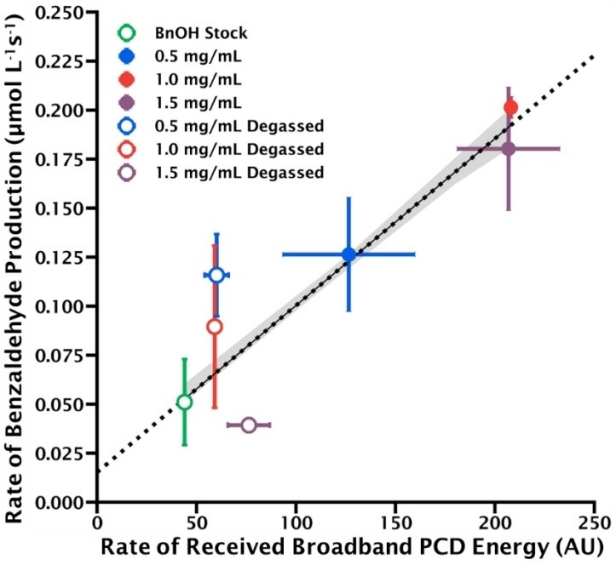

Figure 4. The rate of benzaldehyde production was assessed for various concentrations of (a) freshly-prepared AuPd/TONs and degassed AuPd/TONs, both exposed to 10 minutes of ultrasound at 1.1 MHz, 6.8 MPa, 33% duty cycle, and 45 ms pulse length. A linear regression was used to demarcate the correlation between the rate of broadband PCD signal energy, which is proportional to the rate of inertial cavitation energy, and the rate of benzaldehyde production with increasing particle concentrations. $n = 3$ and $\bar{x} \pm$ SEM, shaded region represents 67% confidence interval for the regression fitting.

for ultrasonic irradiation were selected to minimize thermal effects due to ultrasound over long irradiation times. It was observed that BzA yield increased linearly with time in the presence of PCNs and high frequency ultrasound. The reaction rates were computed from the slopes of the linear regressions and summarized in Table S3. Correspondingly, the estimated turnover frequency (TOF, Figure 5a) of BzA production demonstrated a significant increase with duty cycle, from $0.08 \pm 0.04\ s^{-1}$ (without ultrasound), to $0.34 \pm 0.01\ s^{-1}$ at 5% duty cycle, and finally $1.27 \pm 0.04\ s^{-1}$ at 10% duty cycle, when 1.5 mg/mL AuPd/TONs was used. The degassed AuPd/TONs also exhibited an apparent increase in TOF with increasing duty cycle. However, the reduction in bubble stability (i.e. degassed AuPd/TONs) resulted in substantially lower TOFs (by ~3.9-fold compared to the fresh AuPd/TONs) and a statistically insignificant effect on the rate. For the degassed AuPd/TONs, the marginal increase in rate with duty cycle may be related to secondary acoustic phenomena (e.g., thermal effects) over prolonged ultrasonic irradiation.

Next, we compare the correlations between the cumulative yield of BzA and the total amount of cavitation energy received (as represented by the broadband PCD signal) for systems containing AuPd/TONs, degassed AuPd/TONs or without any cavitation agent, as shown in Figure 5b. Again, the variation in cavitation energy is achieved by varying the concentration of PCNs, duty cycle, and ultrasound irradiation time. As shown in Figure 5b, for all the reaction systems studied, there is generally a positive correlation between the total received cavitation energy and the benzaldehyde yield. Ultrasonic irradiation in the presence

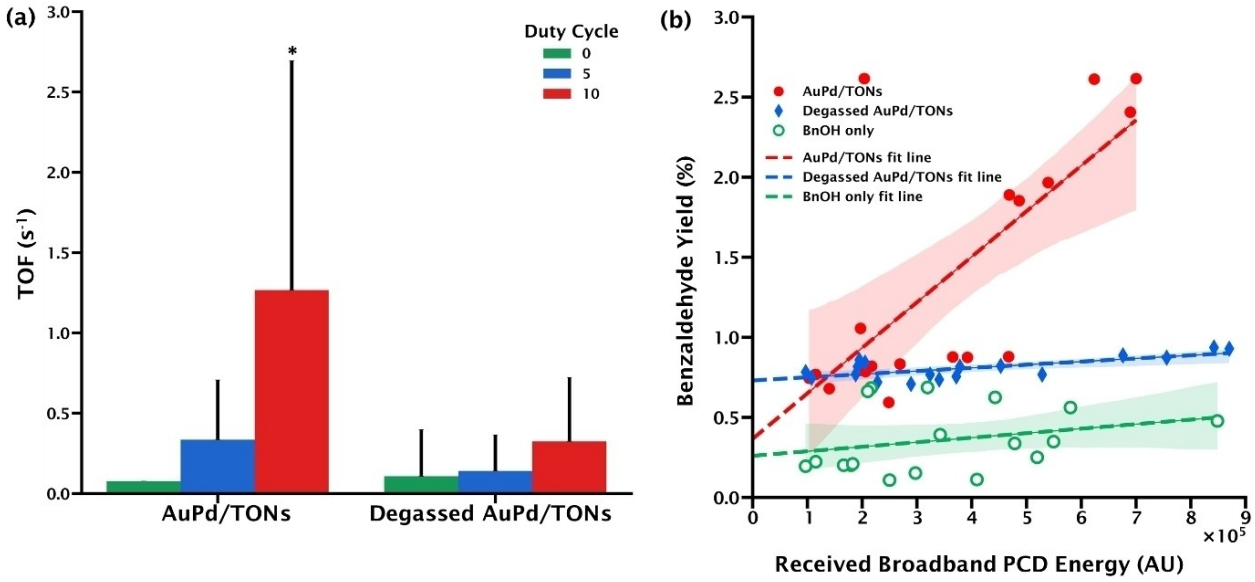

Figure 5. (a) The turnover frequency for PCN-mediated benzaldehyde production was calculated from the rates generated from 0–30 minutes ultrasonic irradiation at different duty cycles (1.1 MHz, 6.8 MPa, 0%–10% duty cycle, and 10 msec pulse length) derived from the Figure S6. (b) The benzaldehyde yield generated at these different stimulation parameters was further correlated against cavitation energy. A linear regression was used to better visualize the relationship between benzaldehyde yield as a function of cavitation energy for a given catalyst group. n = 3, μ ± 67% confidence interval for Figure 5a, 95% confidence interval is shown for the linear regressions in Figure 5b; *$p < 0.05$.

of AuPd/TONs exhibited the greatest correlation between BzA yield and inertial cavitation energy. Comparatively, degassed AuPd/TONs exhibited lower benzaldehyde productivity at similar received inertial cavitation energies. In the absence of any PCN or catalyst, inertial cavitation at comparable intensities yielded the least BzA. Therefore, the results shown in Figure 5b highlight the importance of having gas-stabilizing PCNs for enhanced and sustained inertial cavitation in close proximity to the catalytic active sites to promote the sono-oxidation of benzyl alcohol.

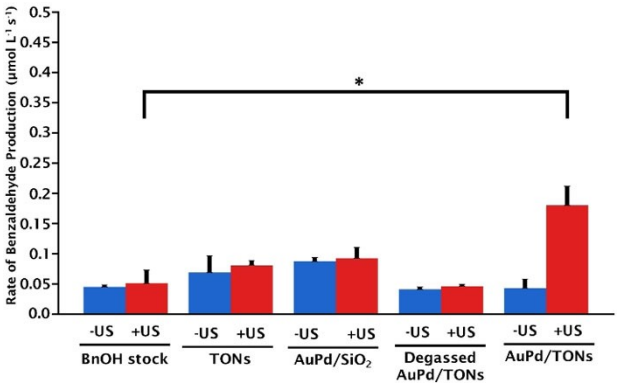

Figure 6. Rates of sonochemical benzaldehyde production using different PCNs in a homogeneous BnOH solution, or in suspensions containing TONs, AuPd/SiO_2, degassed AuPd/TONs or freshly prepared AuPd/TONs. The concentration of cavitation agent/PCNs used in all suspensions is 1.5 mg/ml. The mean rate is presented, and the error bars represent the standard deviation of the sample mean with n = 3. *$p < 0.05$. Acoustic parameters used for + US groups were 1.1 MHz, pulse length 45 ms, duty cycle 33%, 6.8 MPa peak negative pressure. Benzyl alcohol conversion without ultrasound over the same irradiation period is denoted as −US.

The Role of Sonoluminescence

Typically, conventional sonochemical methods utilize continuous wave ultrasound for sonolytic radical generation, which further interacts with reactants and heterogenous catalysts for chemical processing.[2b,5,9,27] It has been well established that sonoluminescence occurs during inertial cavitation,[4d–i] which can interact with photocatalysts for radical generation.[4c,28] Thus, two possible mechanisms existing during the activation of the PCNs. To identify the dominating phenomena, AuPd nanoparticles were loaded onto a photo-inert nanostructure with morphology and particle size similar to that of TONs, viz. SiO_2 nanocups (SEM images shown in Figure S7), forming AuPd/SiO_2, which were examined for the sonochemical oxidation of BnOH to BzA under identical operating conditions. Therefore, the AuPd/SiO_2 sonocatalyst would function solely through sonolysis, without any contribution by sonoluminescence. After 10 min of ultrasound irradiation at 33% duty cycle with 6.8 MPa peak negative pressure, the experiment with AuPd/SiO_2 did not afford a significant increase in the BzA yield compared to the control groups without ultrasound irradiation or cavitation agent, as shown in Figure 6 and Table S4. Therefore, we conclude that sonoluminescence plays an important role in boosting the rate of AuPd/TONs-facilitated sonochemical oxidation of BnOH. Specifically, the TiO_2 in AuPd/TONs is activated by the broadband UV light[29] generated by sonoluminescence and produces charge carriers which helps to drive the catalytic reaction. Without a photoactive cavitation agent, e.g. in the case of AuPd/SiO_2, cavitation-mediated oxidation pro-

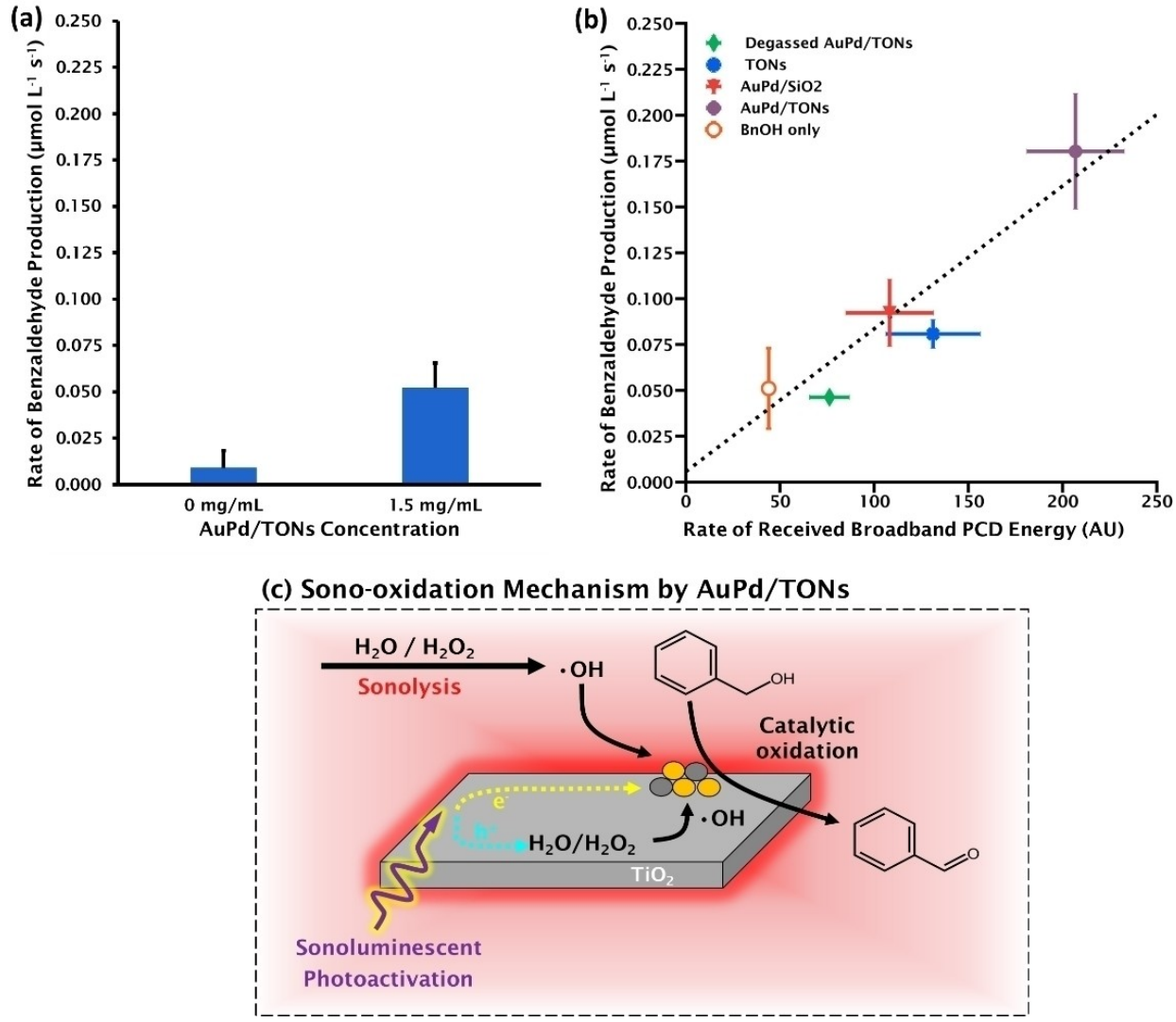

Figure 7. (a) Photo-oxidation performance of AuPd/TONs was evaluated using a dedicated 300 W xenon lamp ($\lambda = 100–2000$ nm). (b) Rates of sonochemical benzaldehyde production with various PCNs after 10 minutes of ultrasonic irradiation (1.1 MHz, 33% duty cycle, 6.8 MPa peak negative pressure) were correlated to the rate of received broadband PCD energy, which is proportional to the inertial cavitation energy. (c) Proposed mechanism for sonochemical oxidation of benzal alcohol using AuPd/TONs. Upon the inertial collapse of the bubble, the sonolysis of water and H_2O_2 generates H• and •OH. Sonoluminescence results in the photoactivation of TiO_2, further generating ROS such as •OH. The supported AuPd nanoparticles functions as charge-carrier separators and active sites for BnOH oxidation to benzaldehyde.

ceeds via other related phenomena, such has surface plasmon resonance, at a significantly slower rate.[20]

Influence of Thermal Effects and Ambient Light as Secondary Stimuli

The contributions by other experimental stimuli, viz. temperature and ambient light were also examined. During ultrasound irradiation, the mechanical energy dissipated by ultrasound heated the reaction mixture[30] up to 44 °C, which eventually stabilized at ~39 °C (Figure S8). This thermal effect was observed in all experiments, regardless of the cavitation response or the reaction rate. In fact, the thermal effect could be responsible for the slight increase in the "background activity" upon ultrasound irradiation (cf. the "−US" experimental group), as shown in Figure 5b and Figure S6. However, the ubiquitous temperature rises in all "+US" experiments could not account for the drastic increase in reaction rate during the sonochemical experiments with AuPd/TONs. In addition, although the AuPd/TONs are photoactive under a xenon lamp (Figure 7a), all acoustic experiments were performed in light-fast tubes to minimize the influence of ambient light. Therefore, any photocatalytic conversion of BnOH could only originate from sonoluminescence light generated upon the inertial collapse of bubbles on the PCNs' surfaces.

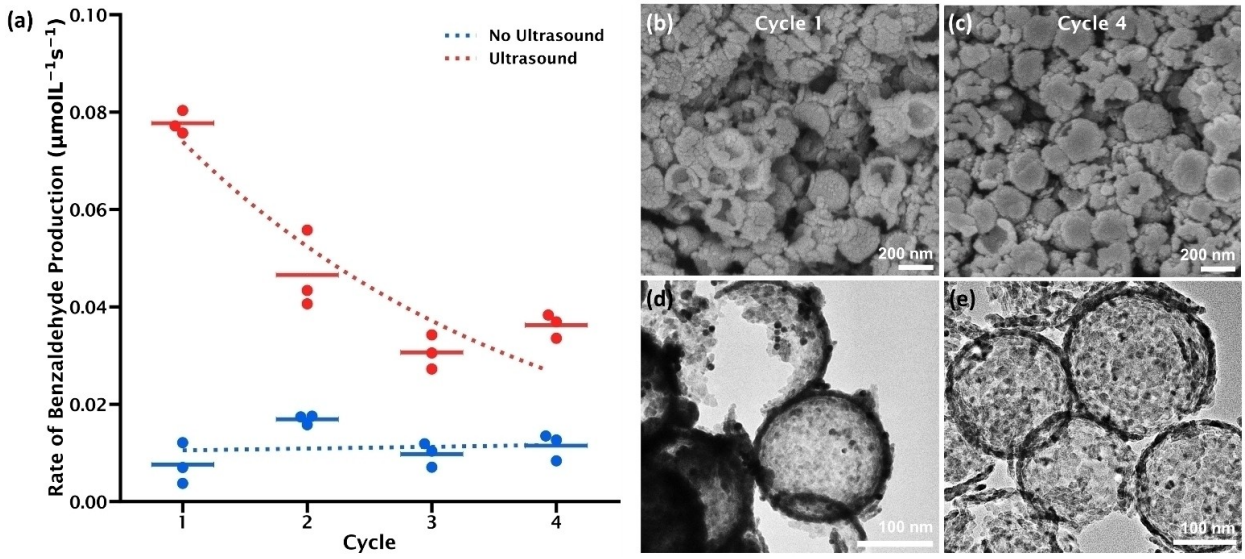

Figure 8. Recyclability of the particles was assessed by successive use and washing cycles. (a) Cycle 1 refers to a stock of fresh particles, which were irradiated with ultrasound, collected, washed, dried and subsequently reused for each successive cycle. Benzaldehyde production rates with AuPd/TONs and ultrasound exposure were compared against PCN solutions without ultrasound as a reference. The horizonal bar is depicted at the mean based on n = 3, exponential decay fit was used to visualize the benzaldehyde yield change from cycle 1 to 4. The morphology of the particles after irradiation at cycle 1 and cycle 4 was assessed by SEM (c, d) and TEM (d, e) to validate fragmentation of the particles and retention of the AuPd co-catalysts, respectively. Scale bars for (b, c) denote 200 nm, (d, e) denote 100 nm. Acoustic parameters used were 1.1 MHz, 10% duty cycle, 10 ms pulse duration, 20 minutes irradiation period, and 6.8 MPa peak negative pressure.

The Role of AuPd Nanocatalyst

The AuPd co-catalysts may play multiple roles during the cavitation-mediated BnOH oxidation. By plotting the rate of reaction against the rate of receipt of cavitation energy, we established a linear correlation between the two quantities across different test groups under identical ultrasound parameters (i.e., 33% duty cycle and 10 minutes of exposure at 6.8 MPa peak negative pressure), as shown in Figure 7b. Remarkably, AuPd/TONs are not only the most efficient cavitation agents for generating inertial cavitation, but also the one showing the highest activity. In contrast, the rates of receipt of inertial cavitation energy and the rate of reactions on bare TON, degassed AuPd/TONs and AuPd/SiO_2 were all significantly lower than those of AuPd/TONs. In fact, under the present test conditions, all cavitation agents other than AuPd/TON showed statistically insignificant improvement in reaction rates over a homogeneous solution under ultrasound irradiation (i.e., "BnOH only"). Therefore, the AuPd nanoparticles on TONs is crucial for efficiently utilizing the ROS generated for the catalytic oxidation of BnOH.

In summary, the results and discussions above establish the essential functions of the AuPd/TONs during sonochemistry, including (i) nanostructure-stabilized bubbles to trigger inertial cavitation near the (photo)catalytic active sites at relatively low acoustic intensities, (ii) photoactive anatase TiO_2 to generate additional ROS by utilizing sonoluminescence light and (iii) AuPd active sites to utilize the ROS generated for the oxidative conversion of BnOH to benzaldehyde (mechanism illustrated in Figure 7c). It has been reported that Au co-catalysts facilitate dehydrogenation of alcohols to aldehydes, while Pd co-catalysts can generate ROS by oxygen reduction.[31] The alloying of the metals has been demonstrated to synergize these functions to promote ROS generation to propagate selective oxidation of benzyl alcohol to benzaldehyde.[31a,32] Despite this, we observed minimal catalytic activity by AuPd/TONs to oxidize benzyl alcohol without ultrasound irradiation over 30 minutes. As the cavitation events result in various chemical, mechanical, and thermal effects, which can drive the reaction forward, our present findings indicate that ultrasound and co-localization of the inertial cavitation events on the catalysts promote oxidation of alcohol to aldehyde. However, further investigations are needed to isolate and probe the key factors influencing the AuPd/TONs-catalyzed sonochemistry.

Recyclability of AuPd/TONs

To verify the practicality of using AuPd/TONs as sonocatalysts, their performance was evaluated over 4 successive batch experiments, each referred as a cycle (Figure 8a). In each cycle, the reaction mixture was subjected to 20 min ultrasonic irradiation at a 10% duty cycle. At the end of each cycle, the catalyst was collected, washed, and oven-dried overnight at 65 °C for use in the next cycle. Figure 8a shows that, following an initial decay over the first 2 cycles, the catalyst activity had stabilized by Cycle 3, showing a rate of BzA production of 0.04 μmol L^{-1} s^{-1}, which is still 2.7 times higher than the background activity of 0.015 μmol L^{-1} s^{-1}. Here, the initial deactivation may be due to morphological changes, as suggested by the particle fragmentation seen in

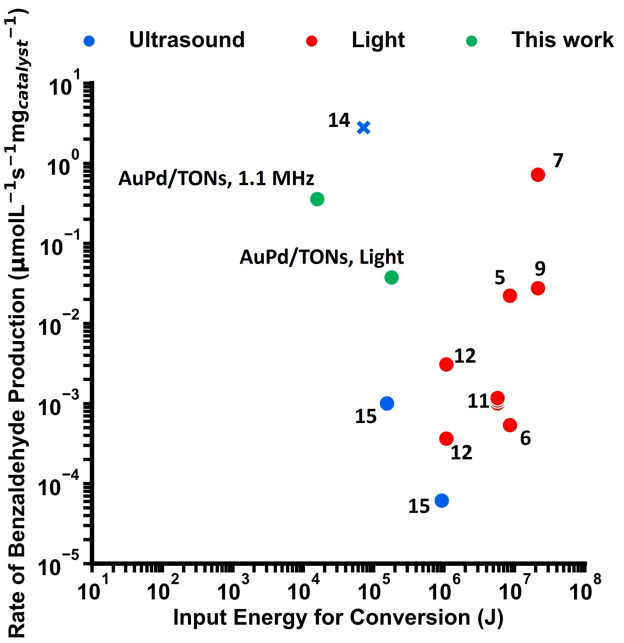

Figure 9. Rate of benzaldehyde production versus energy consumption by the various sono- and photo-catalytic systems reported in the literature and the current work (using AuPd/TONs). The numbered data entries correspond to the references cited in Supplementary Tables S5 and S6, which also showed the detailed reaction data. Data entries of homogenous catalyst reactions are denoted by (X), while the experiments with heterogeneous catalysts are denoted by closed circles.

Figure 8b and Figure 8c. Such particle fragmentation may alter the particle surface and result in loss of AuPd, or deterioration in their ability to stabilize bubbles and promote inertial cavitation. We observed that AuPd nanoparticles remained on the surface of the cycled AuPd/TONs, as shown in Figure 8d and Figure 8e. However, some reduction in the AuPd loading was observed between the sample after 1 cycle and 2 cycles, as shown in Table S1. This loss in metal loading may be attributed to chemical leaching and, or attrition due to acoustic phenomena, and is partly responsible for the apparent decrease in catalyst activity over cycles, as shown in Figure 8. Nevertheless, the AuPd nanoparticles were largely preserved on the recycled catalysts, which show considerable residual activity after 4 reaction cycles. Future work should address the issues of particle stability by both optimizing the operation conditions and improving the design of the PCNs.

Energy Efficiency of the PCN-mediated Sonochemistry

A key advantage of using PCNs for sonochemistry is their ability to facilitate sonocatalytic reactions in low-intensity acoustic fields, which do not yield chemical reaction in conventional sonochemical conditions, thus achieving significant energy saving and enhances the energy efficiencies of sonochemistry driven by inertial cavitation. Accordingly, we compare our novel PCN-mediated sonochemistry approach against other light- and ultrasound-based benzaldehyde oxidation studies in the literature, as shown in Tables S5 and S6, respectively. Notably, the mass-normalized reaction rates ($\mu mol\,L^{-1}\,s^{-1}\,mg_{catalyst}^{-1}$) obtained in the present study are on-par with the best heterogeneous systems reported in the literature (Figure 9). Figure 9 shows that AuPd/TONs are capable of significantly reducing the energy requirement whilst achieving the reaction rates that are comparable or even higher than those of conventional light and ultrasound-based methods. In other words, our sonochemistry approach renders substantially improved energy efficiency.

Conclusion

Through a systematic investigation, we show that AuPd/TONs offer three essential functions of photocatalytic nanostructures: (i) enhancing spatially controlled inertial cavitation in close proximity to the photo- and catalytic-active sites, (ii) facilitate the generation free radicals under low-intensity pulsed ultrasound irradiation and (iii) catalyzing benzyl alcohol oxidation. The unique nanostructure and surface properties of AuPd/TONs enabled effective bubble trapping and stabilization, localizing inertial cavitation near the photoactive sites as well as the catalytic active sites upon ultrasound exposure at low acoustic intensities, such that the acoustic energy input could be efficiently utilized for driving sonochemistry. With this novel approach, we demonstrated remarkably improved rates of oxidation of benzyl alcohol to benzaldehyde over 30 minutes of pulsed high frequency ultrasound irradiation. When the bubble stabilization on AuPd/TONs were chemically neutralized (degassed), the acoustic response and sonoactivity of the degassed PCNs were significantly reduced, indicating the importance of gas stabilization for efficient sonochemistry. Without AuPd/TONs and when utilizing other PCNs comprising of different materials, we had similarly observed a reduction in the sonochemical production rate of benzaldehyde, further attributing AuPd/TONs in cavitation-mediated catalysis of benzyl alcohol to benzaldehyde. Given that existing photo-sonochemical approaches to oxidize BnOH require much more intense irradiations over longer times, our PCN-based approach shows promise in reducing the energy burden of sonochemical processes. By quantifying the cavitation energy emitted by PCNs following different modifications, our findings also present the key design elements for developing an effective PCN, enabling future works to explore the versatility of PCNs for a wide range of chemical applications.

Experimental Section

AuPd/TONs Synthesis: All chemicals used in synthesis of PCNs were used as purchased. TiO_2 open nanoshells (TONs) were first prepared by sol-gel template synthesis as described previously.[16,33] In brief, 10 wt% polystyrene (PS) particles (300 nm, PL6003 Agilent, USA) were dispersed in absolute alcohol (107017 Millipore, 10 mL) to afford a 1 wt% PS solution and sonicated for 10 minutes. The solution was then stirred at 800 RPM while titanium butoxide (244112 Sigma, 4 mL, 40 mg/mL in ethanol) was added dropwise to the mixture. This solution was then sealed and stirred for 2 hours at room temperature. Afterwards, the particles were washed and recovered by centrifugation at 4000 RCF for 10 minutes. The

particles were redispersed in ethanol and the washing was repeated a subsequent two times to purify the titanium hydroxide-coated particles. The purified particles were dried up to overnight at 60 °C to remove residual solvent prior to calcination (5 °C/min temperature ramp) at 500 °C for 3 hours, followed by air cooling to ambient temperature. The particles were then collected and stored in a dry cabinet at 30% humidity for future use.

Following calcination, TONs were surface deposited with AuPd nanoparticles (AuPd/TONs) to validate their performance as a support structure with other nanomaterials for specific chemical reactions. Au nanoparticles (NPs) were synthesized first, followed by alloying of Pd into Au NPs. In a typical procedure, 5 mL of oleylamine (OLAM, 70%, Sigma-Aldrich) was degassed under flowing Argon at 150 °C in a 50 mL flask. 0.3 mmol of $HAuCl_4 \cdot 3H_2O$ (99%, Sigma-Aldrich) was dissolved in 3 mL OLAM and the mixture was quickly injected into the hot OLAM solution, resulting a solution color change to dark purple. The heating was continued for 1.5 h before the particles precipitated with 50 mL of ethanol, followed by centrifugation at 11000 rpm for 5 min. AuPd NPs were synthesized using a modified seed-mediated process.[17b] A mixture of Au NPs (30 mg) in hexane, OLAM (30 mL), oleic acid (1.9 mL, Sigma-Aldrich), and $Pd(NO_3)_2 \cdot 2H_2O$ (15 mg, Sigma-Aldrich) was heated to 140 °C under flowing Argon in a 100 mL flask, and stirred for 30 min. The solution was cooled to room temperature and AuPd NPs were collected by precipitation and centrifugation for three times using isopropanol (5 mL) and ethanol (25 mL). AuPd NPs were loaded onto the TONs surface by slowly adding a solution of AuPd NPs in 3 mL hexane to the dispersion of TONs in 27 mL ethanol. The solution was stirred for 2 hours in ambient conditions in a closed vial. The resulting particles were recovered by centrifugation and dried at 70 °C prior to further use.

For preparation of degassed AuPd/TONs, a known mass of AuPd/TONs particles were dispersed in ethanol overnight, after which the ethanol was removed by centrifugation for 10 minutes at 10000 RCF. The particle pellet was resuspended in aqueous media (either water or 500 ppm BnOH in water) to repeat the washing a subsequent two times. After the last wash, the particles were resuspended in aqueous media at a concentration of 0.5, 1, or 1.5 mg/mL.

For recycling studies, microcentrifuge tubes containing the AuPd/TONs following ultrasonic irradiation were filled with ethanol and then bath sonicated for 5 minutes to thoroughly mix the particles. The solutions were then transferred to a 50 mL conical tube and washed at 10000 RCF for 5 minutes, then redispersed in 10% hexane in ethanol and washed a subsequent two times before drying overnight at 70 °C.

PCN Characterization: The crystal structure of the TONs particles was examined by X-ray diffraction (Bruker D2 Phaser) by Cu Kα radiation with an accelerating voltage and current at 30 kV and 10 mA, respectively. The phase angle was adjusted between 5° and 40° at 0.05° increments ($2\Theta = 10–80°$) with a scan time of 0.5 seconds at each step.

The morphology of the particles was confirmed by field emission scanning electron microscopy (FE-SEM, JEOL JSM-6700, Japan) at an acceleration voltage of 5 kV and transmission electron microscopy (TEM, JEOL JEM-1400, Japan) was performed operating at 120 kV.

Inductively coupled plasma – optical emission spectrometry (ICP-OES, Agilent 5800) was used to determine the metal loading. Standard solutions were prepared by stepwise dilution of Au and Pd single element standard (1000 mg/L, Sigma-Aldrich). The loaded Au and Pd in 10 mg accurately weighed sample was digested using 10 mL of aqua regia, and the solution was filtered and diluted to 50 mL in a volumetric flask.

Sono-oxidation of Benzyl Alcohol solutions: The 4.8 mM benzyl alcohol stock solution was prepared by mixing 50 μL benzyl alcohol (402834, Sigma-Aldrich) in 100 mL of distilled water overnight. From this, 25 mL of the stock solution was mixed with 5 mole equivalents of hydrogen peroxide (31 wt%) to give the working solution. AuPd/TONs particles were weighed into light fast Eppendorf tubes and crushed into a fine powder prior to mixing with 1 mL of the working solution. The particle concentration within the tube varied between 0.5–1.5 mg/mL, depending on the study performed. The particle suspension was then placed in a sonicating water bath for 5 seconds further disperse the particles. The acoustic focus was set within the lumen of the tube at the 0.5 mL mark prior to ultrasound irradiation. A conventional HIFU setup was used in all HIFU experiments, and details of the setup are found in other reports (Figure S10).[14,34] Irradiation parameters were set to 45 msec pulse duration and a 33% duty cycle and 10 minutes irradiation. For our time series experiments (0–30 minutes), the pulse duration was reduced to 10 msec and we utilized a series of duty cycles from 0–10% to minimize heat transfer to the reaction chamber.

Quantification of Benzaldehyde Yield: After selective oxidation by light or ultrasound, particles were filtered from solution by centrifugation at 10000 RCF for 10 minutes. The supernatant was extracted and its contents were quantified by GC-MS (Agilent 5973N GCMS) using a DB5 column. The injector temperature was set to 220 °C and the oven was set to hold at 170 °C for 1 minute, then ramp to 180 °C at a 1 °C/min heating rate. The elution (1 μL) was injected into the GC and perfused through the column at a rate of 0.8 mL/min using helium as the carrier gas. The ion content of the sample was quantified by mass spectroscopy using a scan from 20–220 m/z. The resulting total ion chromatography (TIC) plot was processed through a custom MATLAB script to calculate the area under the product (A_{BnA}) and reactant (A_{BnOH}) curves. A standard curve was used to correlate the product area to molar yield (Figure S11), from which all subsequent measurements were evaluated from.

Statistical Analysis: Where relevant, statistical analysis was performed by one-way analysis of variance (ANOVA) with post hoc analysis done by Tukey's multiple comparisons test to find the p-values between groups. Statistical difference was measured when the p-value between the negative control (e.g., BnOH only either with or without ultrasound) and experimental group was less than 0.05. All p-values are listed in the associated supplementary tables (Table S2–4). For plots correlating either cavitation energy or ultrasound irradiation time to benzaldehyde yield, an ordinary least squares linear regression model was used. From the slope of this model for time vs yield data, the reaction rates were then calculated, and the turnover frequency was subsequently calculated from the reaction rates by normalizing to the moles of AuPd co-catalyst. The confidence intervals for all regression lines were calculated from Python at 67% or 95%.

Acknowledgements

The authors thanks Assoc. Prof Xu Rong and Shuyang Wu for use of their xenon lamp. JJK acknowledges financial support from the Start-up Grant of Nanyang Technological University (M4081814.120). WL acknowledges financial support by the Start-up Grant of Nanyang Technological University, the National Research Foundation, Singapore under its Campus for Research Excellent and Technological Enterprise (CREATE) programme, and the NRF-ANR Joint Research Project (NRF2020-NRF-ANR066 SonoNanoCat).

Conflict of Interest

The authors declare no conflict of interest.

Data Availability Statement

The data that support the findings of this study are available from the corresponding author upon reasonable request.

Keywords: Sonochemistry · cavitation · sonoluminescence · selective oxidation

[1] a) K. S. Suslick, J. R. BlakePerutz, Y. Didenko, M. M. Fang, T. Hyeon, K. J. Kolbeck, W. B. McNamara, M. M. Mdleleni, M. Wong, *Philos. Collect. R. Soc. London, Ser. A* **1999**, *357*, 335–353; b) H. Xu, B. W. Zeiger, K. S. Suslick, *Chem. Soc. Rev.* **2013**, *42*, 2555–2567.
[2] a) K. S. Suslick, G. J. Price, *Annu. Rev. Mater. Sci.* **1999**, *29*, 295–326; b) T. G. McKenzie, F. Karimi, M. Ashokkumar, G. G. Qiao, *Chemistry* **2019**, *25*, 5372–5388.
[3] D. Meroni, R. Djellabi, M. Ashokkumar, C. L. Bianchi, D. C. Boffito, *Chem. Rev.* **2021**, *122*, 3219–3258.
[4] a) R. J. Wood, J. Lee, M. J. Bussemaker, *Ultrason. Sonochem.* **2017**, *38*, 351–370; b) R. G. Thomas, U. S. Jonnalagadda, J. J. Kwan, *Langmuir* **2019**, *35*, 10106–10115; c) J. Bogdan, J. Plawinska-Czarnak, J. Zarzynska, *Nanoscale Res. Lett.* **2017**, *12*, 225; d) M. A. Beckett, I. Hua, *J. Phys. Chem. A* **2001**, *105*, 3796–3802; e) E. Beguin, S. Shrivastava, N. V. Dezhkunov, A. P. McHale, J. F. Callan, E. Stride, *ACS Appl. Mater. Interfaces* **2019**, *11*, 19913–19919; f) M. P. Brenner, S. Hilgenfeldt, D. Lohse, *Rev. Mod. Phys.* **2002**, *74*, 425–484; g) M. A. Margulis, I. M. Margulis, *Ultrason. Sonochem.* **2002**, *9*, 1–10; h) K. S. Suslick, D. J. Flannigan, *Annu. Rev. Phys. Chem.* **2008**, *59*, 659–683; i) T. J. Matula, R. A. Roy, *Ultrason. Sonochem.* **1997**, *4*, 61–64.
[5] J. Collins, T. G. McKenzie, M. D. Nothling, M. Ashokkumar, G. G. Qiao, *Polym. Chem.* **2018**, *9*, 2562–2568.
[6] a) Y. He, J. Wan, Y. Yang, P. Yuan, C. Yang, Z. Wang, L. Zhang, *Adv. Healthcare Mater.* **2019**, *8*, e1801254; b) X. Wang, X. Zhong, L. Bai, J. Xu, F. Gong, Z. Dong, Z. Yang, Z. Zeng, Z. Liu, L. Cheng, *J. Am. Chem. Soc.* **2020**, *142*, 6527–6537; c) X. Zhong, M. Zhang, Z. Tian, Q. Wang, Z. Wang, *Nanoscale Res. Lett.* **2019**, *14*, 381.
[7] M. Pappaterra, P. Xu, W. van der Meer, J. A. Faria, D. Fernandez Rivas, *Ultrason. Sonochem.* **2021**, *70*, 105324.
[8] H. Mohapatra, M. Kleiman, A. P. Esser-Kahn, *Nat. Chem.* **2017**, *9*, 135–139.
[9] T. G. McKenzie, E. Colombo, Q. Fu, M. Ashokkumar, G. G. Qiao, *Angew. Chem. Int. Ed. Engl.* **2017**, *56*, 12302–12306.
[10] T. Leong, M. Coventry, P. Swiergon, K. Knoerzer, P. Juliano, *Ultrason. Sonochem.* **2015**, *27*, 22–29.
[11] Y. Wang, Y. Xu, S. Dong, P. Wang, W. Chen, Z. Lu, D. Ye, B. Pan, D. Wu, C. D. Vecitis, G. Gao, *Nat. Commun.* **2021**, *12*.
[12] a) Y. L. Pang, S. Lim, R. K. L. Lee, *Environ. Sci. Pollut. Res. Int.* **2020**, *27*, 34638–34652; b) S. Liang, X. Deng, G. Xu, X. Xiao, M. Wang, X. Guo, P. a. Ma, Z. Cheng, D. Zhang, J. Lin, *Adv. Funct. Mater.* **2020**, *30*.
[13] E. Beguin, M. D. Gray, K. A. Logan, H. Nesbitt, Y. Sheng, S. Kamila, L. C. Barnsley, L. Bau, A. P. McHale, J. F. Callan, E. Stride, *J. Controlled Release* **2020**, *317*, 23–33.
[14] a) J. J. Kwan, R. Myers, C. M. Coviello, S. M. Graham, A. R. Shah, E. Stride, R. C. Carlisle, C. C. Coussios, *Small* **2015**, *11*, 5305–5314; b) X. Su, R. G. Thomas, L. D. Bharatula, J. J. Kwan, *Sci. Rep.* **2019**, *9*, 9612.
[15] a) J. Wang, Y. Guo, B. Liu, X. Jin, L. Liu, R. Xu, Y. Kong, B. Wang, *Ultrason. Sonochem.* **2011**, *18*, 177–183; b) D. G. You, V. G. Deepagan, W. Um, S. Jeon, S. Son, H. Chang, H. I. Yoon, Y. W. Cho, M. Swierczewska, S. Lee, M. G. Pomper, I. C. Kwon, K. Kim, J. H. Park, *Sci. Rep.* **2016**, *6*, 23200.
[16] U. S. Jonnalagadda, X. Su, J. J. Kwan, *Ultrason. Sonochem.* **2021**, *73*, 105530.
[17] a) D. I. Enache, J. K. Edwards, P. Landon, B. Solsona-Espriu, A. F. Carley, A. A. Herzing, M. Watanabe, C. J. Kiely, D. W. Knight, G. J. Hutchings, *Science* **2006**, *311*, 362–365; b) C. J. Wrasman, A. Boubnov, A. R. Riscoe, A. S. Hoffman, S. R. Bare, M. Cargnello, *J. Am. Chem. Soc.* **2018**, *140*, 12930–12939; c) W. Hou, N. Dehm, R. Scott, *J. Catal.* **2008**, *253*, 22–27.
[18] M. L. Chevallier, S. Dessolin, F. Serres, L. Bruyas, G. Chatel, *Molecules* **2019**, *24*.
[19] P. O'Brien, D. Lopez-Tejedor, R. Benavente, J. M. Palomo, *ChemCatChem* **2018**, *10*, 4992–4999.
[20] X. Su, U. S. Jonnalagadda, L. D. Bharatula, J. J. Kwan, *Ultrason. Sonochem.* **2021**, *79*.
[21] S. K. Khore, S. R. Kadam, S. D. Naik, B. B. Kale, R. S. Sonawane, *New J. Chem.* **2018**, *42*, 10958–10968.
[22] E. Stride, C. Coussios, *Na. Rev. Phys.* **2019**, *1*, 495–509.
[23] B. M. Borkent, S. M. Dammer, H. Schonherr, G. J. Vancso, D. Lohse, *Phys. Rev. Lett.* **2007**, *98*, 204502.
[24] J. Mondal, W. Li, A. R. Rezk, L. Y. Yeo, R. Lakkaraju, P. Ghosh, M. Ashokkumar, *Ultrason. Sonochem.* **2021**, *73*.
[25] a) J. J. Kwan, G. Lajoinie, N. de Jong, E. Stride, M. Versluis, C. C. Coussios, *Phys. Rev. Appl.* **2016**, *6*; b) C. Mannaris, B. M. Teo, A. Seth, L. Bau, C. Coussios, E. Stride, *Adv. Healthcare Mater.* **2018**, *7*, e1800184; c) C. D. Arvanitis, M. Bazan-Peregrino, B. Rifai, L. W. Seymour, C. C. Coussios, *Ultrasound Med Biol* **2011**, *37*, 1838–1852.
[26] C. M. Crombie, R. J. Lewis, R. L. Taylor, D. J. Morgan, T. E. Davies, A. Folli, D. M. Murphy, J. K. Edwards, J. Qi, H. Jiang, C. J. Kiely, X. Liu, M. S. Skjøth-Rasmussen, G. J. Hutchings, *ACS Catal.* **2021**, *11*, 2701–2714.
[27] P. N. Amaniampong, Q. T. Trinh, K. De Oliveira Vigier, D. Q. Dao, N. H. Tran, Y. Wang, M. P. Sherburne, F. Jérôme, *J. Am. Chem. Soc.* **2019**, *141*, 14772–14779.
[28] a) E. Alves Nunes Simonetti, L. D. S. Cividanes, T. M. Bastos Campos, F. Williams Fernandes, J. P. B. Machado, G. P. Thim, *Fullerenes Nanotubes Carbon Nanostruct.* **2015**, *23*, 725–733; b) J.-Y. Jung, D. Lee, Y.-S. Lee, *J. Alloys Compd.* **2015**, *622*, 651–656; c) N. Shimizu, C. Ogino, M. F. Dadjour, T. Murata, *Ultrason. Sonochem.* **2007**, *14*, 184–190.
[29] Y. T. Didenko, S. P. Pugach, *J. Phys. Chem.* **2002**, *98*, 9742–9749.
[30] G. ter Haar, *J. Ultrasound* **1999**, *9*, 3–9.
[31] a) D. I. Enache, J. K. Edwards, P. Landon, B. Solsona-Espriu, A. F. Carley, A. A. Herzing, M. Watanabe, C. J. Kiely, D. W. Knight, G. J. Hutchings, *Science* **2006**, *311*, 362–365; b) P. Landon, P. J. Collier, A. F. Carley, D. Chadwick, A. J. Papworth, A. Burrows, C. J. Kiely, G. J. Hutchings, *Phys. Chem. Chem. Phys.* **2003**, *5*, 1917–1923.
[32] a) G. Li, D. I. Enache, J. Edwards, A. F. Carley, D. W. Knight, G. J. Hutchings, *Catal. Lett.* **2006**, *110*, 7–13; b) Y. Liu, Y. Wang, W. Zhen, Y. Wang, S. Zhang, Y. Zhao, S. Song, Z. Wu, H. Zhang, *Biomaterials* **2020**, *251*; c) X. Huang, O. Akdim, M. Douthwaite, K. Wang, L. Zhao, R. J. Lewis, S. Pattisson, I. T. Daniel, P. J. Miedziak, G. Shaw, D. J. Morgan, S. M. Althahban, T. E. Davies, Q. He, F. Wang, J. Fu, D. Bethell, S. McIntosh, C. J. Kiely, G. J. Hutchings, *Nature* **2022**, *603*, 271–275.
[33] J. Wang, J. Yu, X. Zhu, X. Z. Kong, *Nanoscale Res. Lett.* **2012**, *7*, 646.
[34] U. S. Jonnalagadda, T. M. Nguyen, F. Li, J. H. C. Lee, X. Liu, A. Goto, J. J. Kwan, *Macromol. Chem. Phys.* **2020**, *221*, 2000088

Manuscript received: June 7, 2022
Revised manuscript received: July 24, 2022
Accepted manuscript online: August 15, 2022
Version of record online: October 7, 2022